Progress In Electromagnetics Research M, Vol. 37, 95–107, 2014

On the Scanning Properties of Imaging Antennas Based on Dual Confocal Paraboloidal Reflectors

Fabio Pelorossi[1, 2, 3, *], Giovanni Toso[1], and Piero Angeletti[1]

Abstract—In this paper the scanning properties of dual reflector antenna systems constituted by two confocal paraboloidal reflectors fed by a planar array are investigated. This antenna architecture combines the interesting features of reflectors and array antennas. Because of the offset configuration the radiation pattern exhibits an anomalous deviation in the beam pointing when the beam is scanned out of the boresight direction. Heuristic equations, representing an extension of the linear equations available in the literature, are derived, which permit predicting the pointing direction of the overall system as a function of the pointing direction of the feeding array in a significant field of view.

1. INTRODUCTION

Dual reflector antenna systems constituted by two confocal offset paraboloids fed by a planar array have been probably introduced by Fitzgerald [1]. Later on Dragone et al. [2–4] has further analyzed this antenna system deriving some design rules. After the work of Pearson [5], the Gregorian co-focal dual reflector system, to which we refer also as Dragonian configuration, has been considered as a promising antenna configuration for satellite payloads [6, 7].

The Dragonian antenna, which is an imaging antenna system, combines the interesting features of both reflectors (i.e., focalization properties, low cost, large frequency bandwidth) and array antennas (i.e., electronic pointing and re-configurability). In practice, an array with limited extension together with a dual reflector system, constituted by two confocal paraboloid reflectors, is able to approximate the performance of a large array with an aperture similar to the one of the main reflector. While the equivalent large array antenna exhibits better radiative performance, the imaging antenna system is significantly simpler and cheaper and for this reason it may be considered especially when large antenna apertures and limited scanning capabilities are required [8]. Array excitations techniques may be used to compensate possible distortions of the reflector antenna surface caused by manufacturing tolerances or ageing [7], beside the scanning deviation caused by the offset configuration.

In this paper the scanning performance of this antenna system are analyzed in detail. Special emphasis is placed on the non-linear relations linking the scanning characteristics of the feeding array to the scanning properties of the entire antenna system. These non-linear deviations are caused by the offset configuration.

Figure 1 shows the cross section, in the elevation off-set plane, of a Dragonian system.

Considering a transmission mode, the sub-reflector is able to convert a plane wave, emerging from a planar array, into a spherical wave centered in the common focus while the main reflector re-converts the spherical wave into a plane wave with magnified transverse cross-section. For reciprocity, the transformations are the same in the receive mode case. The increase in the antenna gain, with respect to the isolated feed array, offered by the dual reflector system depends on the magnification ratio, M, which may be defined as the ratio of the focal length of the main reflector f_m to the sub-reflector f_s

Received 31 March 2014, Accepted 20 June 2014, Scheduled 29 June 2014

* Corresponding author: Fabio Pelorossi (fabio.pelorossi@esa.int).

[1] European Space Agency ESA-ESTEC, Noordwijk, The Netherlands. [2] European Space Agency ESA-ESOC, Darmstadt, Germany. [3] Università di Roma La Sapienza, DIET, Roma, Italy.

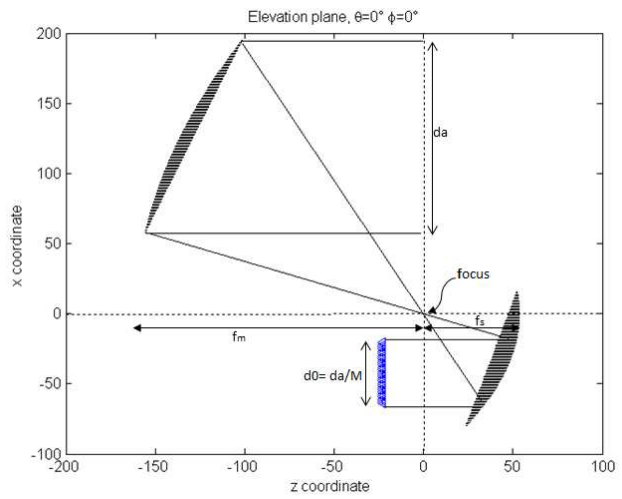

Figure 1. View on the elevation plane of the Dragonian system.

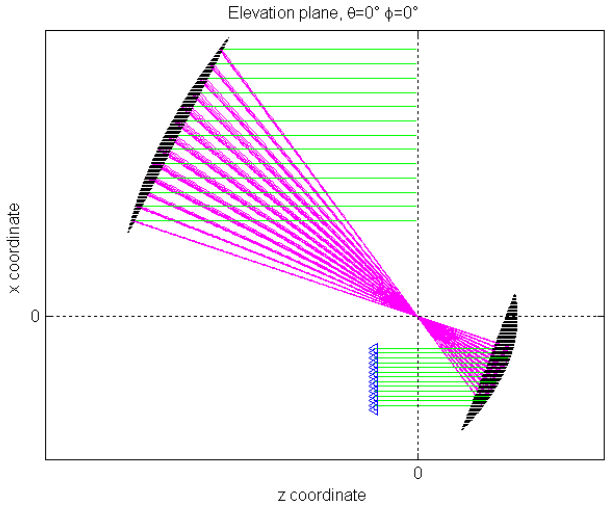

Figure 2. Ray tracing geometrical optics (GO) representation, in the offset plane, of the magnification properties when the array is pointing in the boresight direction.

or as the ratio of the main reflector aperture size d_a to the array aperture dimension d_0 (the second definition being more general because applicable to the case of shaped reflectors as well). Thus, the magnification factor is:

$$M = \frac{d_a}{d_0} = \frac{f_m}{f_s} \tag{1}$$

The optical magnification factor transforms the original feed array into an equivalent feed system where all the geometrical properties are magnified.

As a rule of thumb, the main beam emerging from the main reflector is approximately M times narrower, i.e., M times more directive, as compared to the main beam transmitted or received by the feeding array. Furthermore, if θ and ϕ denote the coordinates which define the pointing direction of the main beam emerging from the array, while θ' and ϕ', are the corresponding directions relevant to the main beam emerging from the main reflector (i.e., the main beam of the entire antenna) then, for a symmetric configuration would be:

$$\begin{aligned} \phi' &= \phi + \pi \\ \theta' &= \frac{f_s}{f_m}\theta = \frac{1}{M}\theta \end{aligned} \tag{2}$$

The accuracy of Equation (2) decreases when increasing the scanning angles and the main objective of this paper consists in deriving a heuristic non-linear extension for these equations.

When scanning the beam originated by the feeding array with respect to the reflectors common axis, the reflected rays originated from the first reflection on the sub-reflector are not perfectly focused anymore in a single point but on a distributed caustic region which moves up or down depending on the direction of scanning (see Figures 3 and 4).

In particular, when the array is scanning up, the main reflector is scanning down and the caustic region moves from the focal point towards the top (Figures 3(a) and 3(b)). Viceversa, when the array is scanning up, the main reflector is scanning down and the caustic region moves down from the focal point getting closer to the array (Figures 4(a) and 4(b)).

Scanning the beam emerging from the feeding array by a certain angle with respect to the boresight direction (coinciding with the direction of the axis of the two confocal paraboloids), corresponds to a tilt of the pattern of the entire antenna roughly M times smaller and in the opposite elevation direction. In addition, the pattern associated to the main reflector is about M times more directive as compared to the pattern generated by the feeding array. However, as already mentioned, the linear Equation (2)

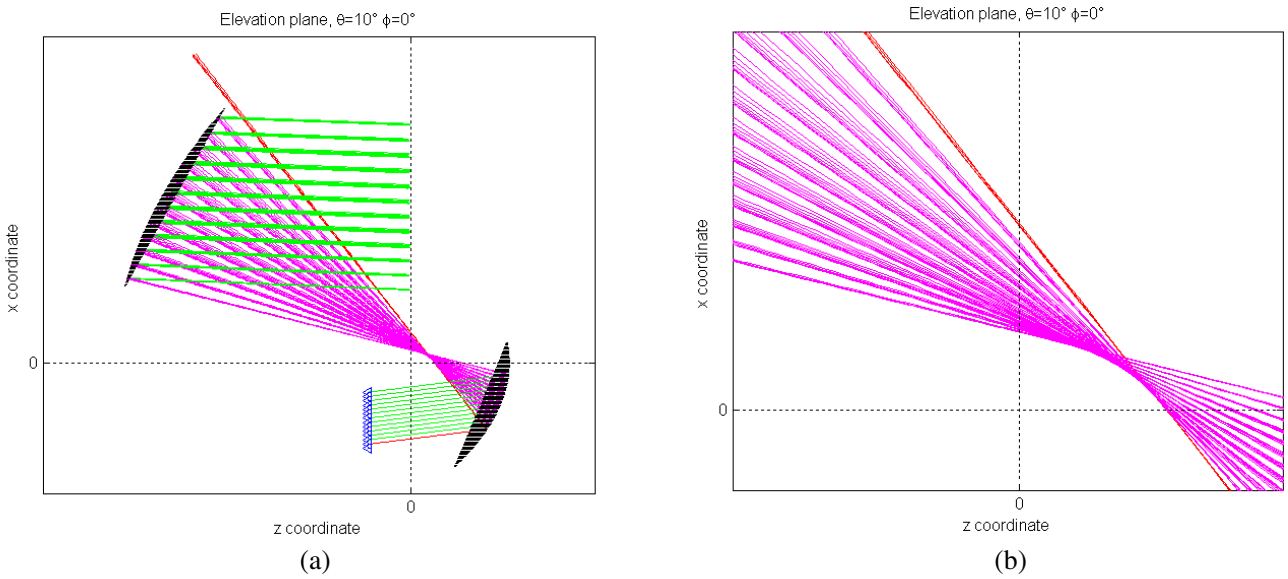

(a) (b)

Figure 3. (a) Ray tracing geometrical optics (GO) representation, in the offset plane, of the magnification properties when the array is scanning 10° up. Spill-over is underlined. (b) Zoom around the distributed caustic region.

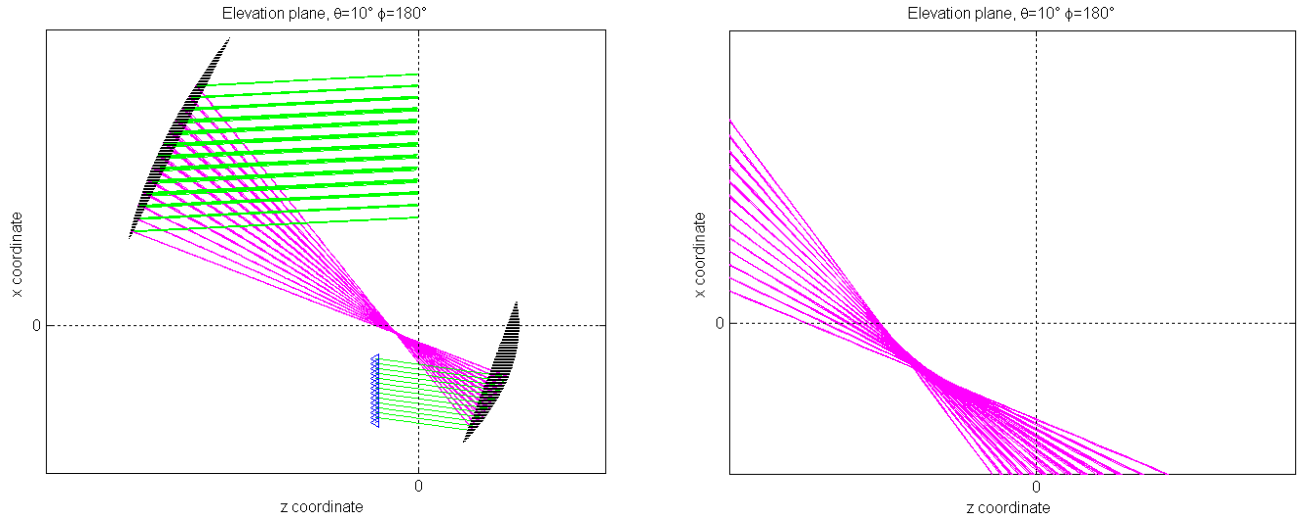

(a) (b)

Figure 4. (a) Ray tracing geometrical optics (GO) representation, in the offset plane, of the magnification properties when the array is scanning 10° down. (b) Zoom around the distributed caustic region.

are well defining the macroscopic behaviour of the entire antenna system but are accurate only for very small scanning angles with respect to the boresight direction. For beams deflected significantly from the boresight direction, the offset configuration determines what are defined as phase aberrations [4] which will be extensively studied in the next paragraphs.

2. AN HYBRID ANALYSIS BASED ON GEOMETRICAL OPTICS (GO) AND PHYSICAL OPTICS (PO)

In this paragraph, an hybrid procedure based on GO and PO is presented. First of all, the amplitude and phase distribution on the main aperture plane have been evaluated as a function of the known

amplitude and phase distributions on the array aperture resorting to the approximate GO procedure described in [2]. As proposed in [2], the array is divided into a two-dimensional lattice of equally spaced sampling points. The index N sets the number of rays traced, as well as the number of sampling points on the main aperture. This parameter determines the trade-off between computational burden and the accuracy of the computed patterns. For each pair of coordinate points x_0, y_0, and for given θ and ϕ, the coordinates of the reflection points on the two reflectors have been evaluated and used to determine the optical path length L.

The amplitude distribution on the main aperture plane, denoted by $E(x_a(m,n), y_a(m,n))$ is related to the assumed distribution on the array imposing the conservation of energy where m, n are the indices that identify the ray into the square lattice of the array.

Thus, from the energy conservation in a ray tube in GO, the following equation [2] may be derived:

$$\Delta x_0(m,n)\Delta y_0(m,n)\left|E_0\left(x_0(m,n),y_0(m,n)\right)\right|^2 = \Delta x_a(m,n)\Delta y_a(m,n)\left|E_a\left(x_a(m,n),y_a(m,n)\right)\right|^2 \quad (3)$$

where:

$$\begin{aligned}\Delta x_0(m,n) &= x_0(m+1,n) - x_0(m,n)\\ \Delta y_0(m,n) &= y_0(m,n+1) - y_0(m,n)\\ \Delta x_a(m,n) &= x_a(m+1,n) - x_a(m,n)\\ \Delta y_a(m,n) &= y_a(m,n+1) - y_a(m,n)\end{aligned}$$

and $|E_0(x_0(m,n),y_0(m,n))|^2$, $|E_a(x_a(m,n),y_a(m,n))|^2$ represent the radiation densities on the array and on the main aperture, respectively.

$\Delta x_0(m,n)$ and $\Delta y_0(m,n)$, interspaces on the array, are constant quantities since the lattice is regular.

Therefore it is possible, adopting a simple GO procedure, to derive the field distribution on the main aperture from (3):

$$E_a\left(x_a(m,n),y_a(m,n)\right) = \sqrt{\Delta x_a(m,n)\Delta y_a(m,n)}E_0\left(x_0(m,n),y_0(m,n)\right) \quad (4)$$

The far field pattern $P(\theta',\phi')$ is then estimated adopting a PO-like procedure, i.e., by numerically implementing a surface radiation integral:

$$P(\theta',\phi') = \sum_m\sum_n \sqrt{\Delta x_a \Delta y_a}E_0(x_a,y_a)e^{-j\Phi(x_a,y_a)}e^{j2\pi f_m \sin\theta'(x_a\cos\phi' + y_a\sin\phi')} \quad (5)$$

where the dependence of the coordinates to m, n is omitted.

Rays which spilled over either the sub-reflectors or the main reflector are excluded in the ray-tracing portion of the program and do not contribute to define the pattern. It should be noted that, with this procedure, each ray is associated to one squared ray tube.

Furthermore, in order to obtain reasonable computational times, a limited field of view around the expected direction of the main beam's radiation may be selected for the computation and visualization of the antenna pattern. Grating lobes have to be considered: their occurrence and level with respect to the main beam is a critical aspect in this type of study.

3. NUMERICAL METHODS FOR THE ANALYSIS OF THE RADIATIVE PROPERTIES OF THE DRAGONIAN ANTENNA

Today, some commercial tools are available for the analysis of dual reflector antennas. In particular, the software GRASP developed by TICRA (http://www.ticra.com/) is extremely reliable, fast, accurate and it is considered the reference tool for reflector based antennas. Despite the maturity of the GRASP tool, for the present work a numerical hybrid routine based on GO and PO has been implemented in house using MATLAB (http://www.mathworks.de/products/matlab/).

As well known, to characterize the interactions between the array and the sub-reflector and the interactions between the two reflectors, GO is sufficiently accurate and extremely fast. For the far field computation GO is not sufficiently accurate while the PO, based on a GO approximation of the fields on the reflector and on the evaluation of the corresponding radiation integrals, provide accurate results especially for electrically large reflectors.

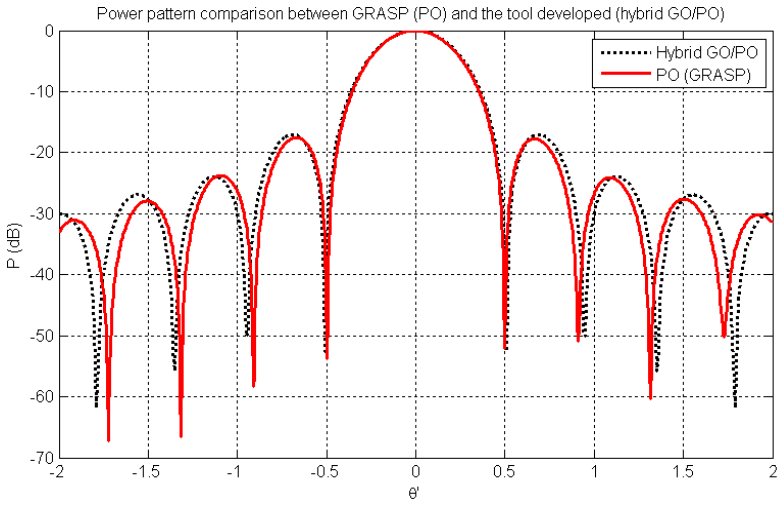

Figure 5. Pattern comparison between GRASP (PO) and a hybrid GO-PO routine in MATLAB.

Figure 5 shows the comparison between far field antenna pattern using the hybrid approach (GO based with rays discretization), implemented in the frame of the present work, and using the GRASP simulation (using a complete PO approximation), for the boresight case.

The matching is quite good, the elaboration time is almost the same, but the software routine developed in house permits to better investigate some system performances in case of scanning, as shown in the following paragraphs.

4. BEAM SCANNING

In this work, a configuration able to generate a 1° first null beam width with a field of view of ±8° (corresponding to a full Earth coverage from a geostationary satellite), is considered as a reference test configuration. Thus, the main circular aperture is selected to have a diameter of 140λ [5] and the positions, as the sizing of the reflectors, have been selected to satisfy the requested scanning capabilities, minimizing blockage and spill-over.

An isolated planar array, to satisfy the same pattern specifications without any reflector antennas, would be slightly smaller but the system would be heavier and more expensive.

The system can be specified as frequency independent. The chosen electrical dimensions correspond to a main reflector of 1.4-meters diameter at 30 GHz.

Moreover, the sub reflector is over-dimensioned more significantly because it is illuminated by the feeding array whose field of view is M times larger as compared to the one of the main reflector.

In particular, due to the offset configuration, the sub-reflector needs a larger oversize in the upper part than in the lower one.

The geometrical parameters characterizing this test configuration are listed hereafter:

Magnification	3
Frequency (GHz)	30
First null beam width (°)	1
Ratio f_s/d_0	1.15
Offset: distance main reflector lower edge from the common axis (cm)	56
Ratio center/focal length for the sub-reflector	0.6
Ratio diameter/focal length for the sub-reflector	1.8
Ratio center of the array/focal length of the sub-reflector	0.79
Distance of the array from the focal plane (cm)	23

As mentioned, when such system is not pointing at the boresight direction, all the rays are not focused on a single focal point but in a distributed caustic region. This leads to a phase aberration, i.e., a deformation of the image produced by the array on the main aperture.

The radiation properties of this antenna system are, as expected, affected by the offset configuration and will be characterized now. Representing a multi-beam coverage, where each beam pattern is computed by scanning the array with steps of 4°, the following figures are obtained, covering the entire desired antenna scan sector of ±8°.

In Figure 6 the plane of scan of the array corresponds to $\phi = 0°$ when the array is scanning down and to $\phi = 180°$ when the array is scanning up (i.e., towards the common focus). As reflected also in Equation (2), when the array is scanning down the main reflector is scanning up and viceversa. So far the pattern is characterized by $\phi' = 180°$ when $\phi = 0°$ and by $\phi' = 0°$ when $\phi = 180°$. Due to the vertical offset, only when the array is scanning in this vertical plane the beam emerging from the array and the corresponding one emerging from the main reflector after two reflections are in the same plane.

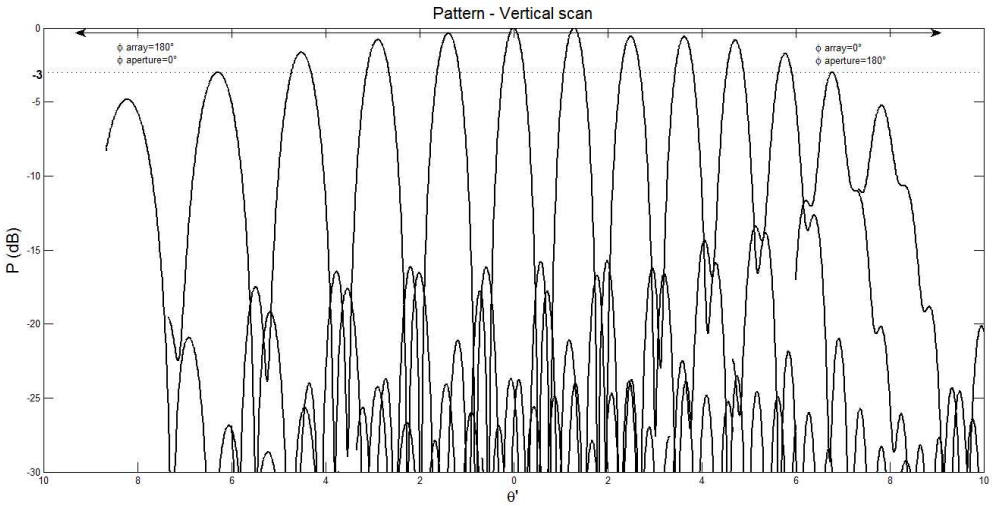

Figure 6. Antenna patterns, on the vertical (x-z) scan plane, with a 4° step on the scanning angles of the feeding array.

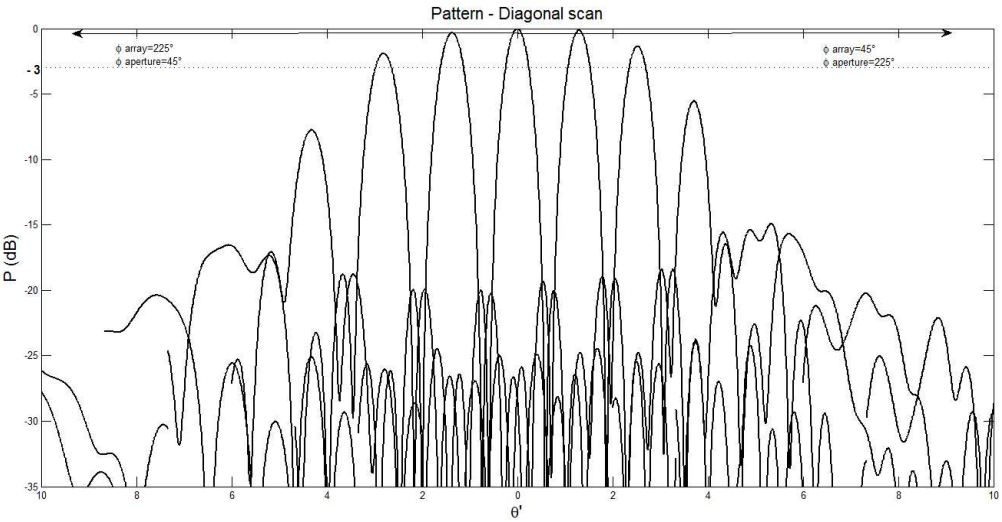

Figure 7. Antenna patterns on the diagonal plane (45°/225°).

In this case, only the θ' direction is affected by the offset configuration, as the system is symmetrical in the y-z plane.

However, in general, when the array is scanning not only in the vertical plane but also in the horizontal one, the relation between the scanning angles of the array and the corresponding ones of the main reflector becomes more complicated. As a consequence, representing the array field and the one emerging from the reflector in the same plane passing through the focus do not permit to visualize exactly the directions of maximum radiation. To clarify this property, let us assume that the array is scanning in the oblique plane characterized by $\phi = 45°$ and $\phi = 225°$. In Figure 7 the corresponding beams emerging from the main reflector are represented in the same oblique plane. Moving from the offset vertical plane, characterized by $\phi = 0°$, $180°$ and $\phi' = 180°$, $0°$, the beams emerging from the main reflector do not have their maxima in the same oblique plane where the array is scanning. So in practice, the results in Figure 7 can be used only to estimate the beam scanning losses in the specific plane where the array is scanning.

5. THE BEAM TRACKING ALGORITHM (BTA)

In order to evaluate the pointing direction of the beam emerging from the main reflector after two reflections, a beam tracking algorithm (BTA) routine has been implemented.

The routine calculates the antenna patterns in all possible directions around the expected one, according to (2), within a selectable range and with a selectable accuracy. The real direction of maximum radiation of the antenna system is then simply associated to the absolute maximum value obtained. The 2D pattern is then calculated replacing the expected angle ϕ' with the angle associated to the direction derived numerically, for every beam. As consequence, in the 2D multibeam representation (e.g., Figure 8, continuous line), the angle ϕ' is different for every beam.

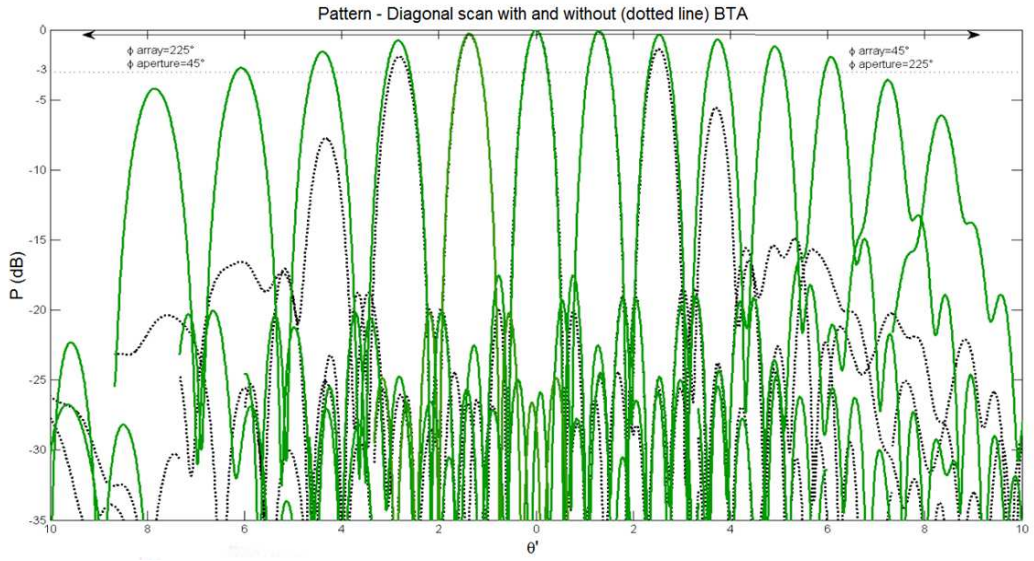

Figure 8. Antenna patterns on the diagonal plane (45°/225°) after BTA correction (in dotted line patterns without BTA).

In particular, Figure 8 shows the beams in the diagonal plane ($\phi = 45°$ and $\phi = 225°$) without using the BTA algorithm (black dotted curves as in Figure 7) and the beams evaluated in their maximum radiation direction as derived by the BTA algorithm (continuous line curves). The accuracy used in the tracking, in this case, is 0.1° for θ' and 0.2° for ϕ'.

It is particularly convenient adopting an orthographic projection of the coordinates ϕ' and θ' to visualize the real scanning behavior underlining the phase aberration for the entire antenna system (Figure 9).

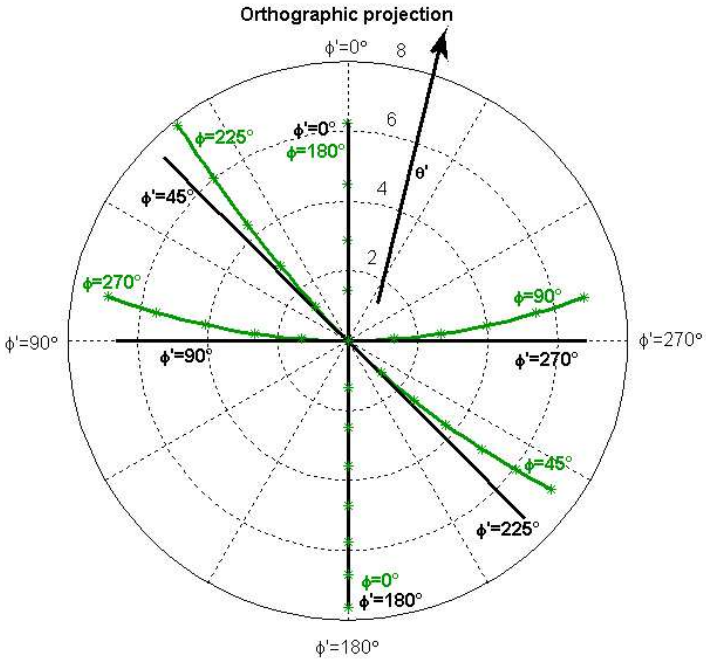

Figure 9. Orthographic projection on the main aperture for 6 test cases. Real patterns directions (curved lines with stars) as compared to ideal scanning directions (straight lines).

In practice, the straight lines in Figure 9 represent the directions where one may expect having the maximum radiation of the beams emerging from the main reflector according to Equation (2). Instead, the curved lines represent the directions where the maxima are effectively located, calculated by the BTA algorithm. So the difference between each couple of lines represents the deformations caused by the offset configuration.

From the orthographic projections it can be also derived that the maximum array scan angle to guarantee 8° of coverage is about 26° in the down vertical scan case from the main aperture, while it is around 21° in the up vertical main scan case. The orthographic projections prove that, despite in the vertical scan case the distortions do not affect the ϕ' angle (but only the elevation angle θ'), in case of oblique scan both angles (θ', ϕ') do not respect both equations in (2), as the scan from the boresight direction is increased. In the limit case of completely horizontal scan (i.e., array scanning in the y-z plane) the distortions affecting both (θ', ϕ') angles are maximized.

In particular, considering θ' for up scanning (upper part of the orthographic circle) there is an expansion of real pointing angles in elevation (respect to the expected ones) along a distorted (curved) plane depending on ϕ'. Otherwise, for down scanning (lower part of the circle) there is a contraction of the θ' angles, respect to the predicted ones. For this reason the two reflectors are oversized asymmetrically.

6. DETERMINATION OF THE ERRORS ON THE PREDICTED DIRECTIONS

Adopting the BTA algorithm is possible to estimate the errors caused by the aberrations on the main beam direction angles. The following figures represent the computed variations between real and expected directions of the main beam, both for θ' and ϕ'.

6.1. Variations on ϕ'

The plot of Figure 10 shows the behavior of the $\Delta\phi'$ function of both θ and ϕ.

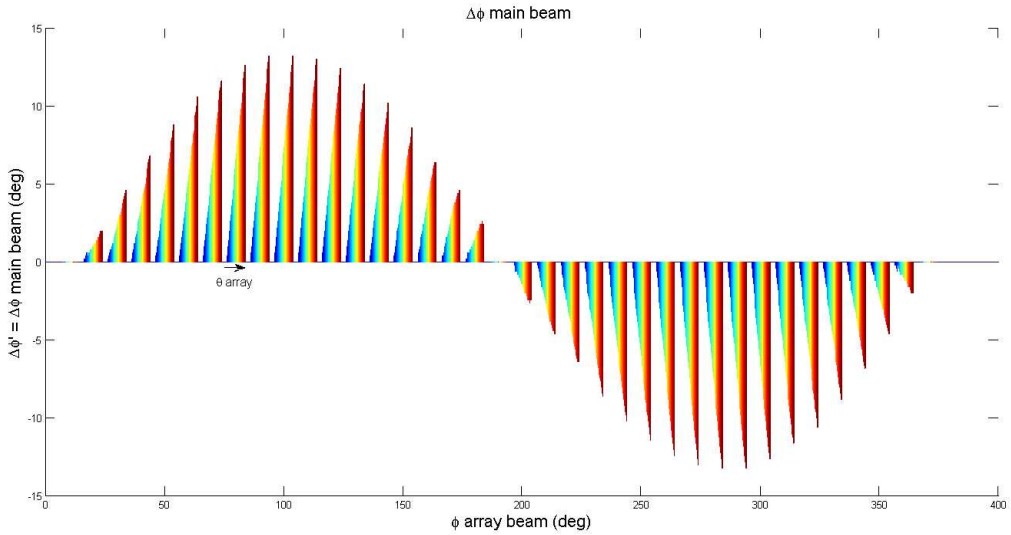

Figure 10. $\Delta\phi'$ as a function of θ and ϕ.

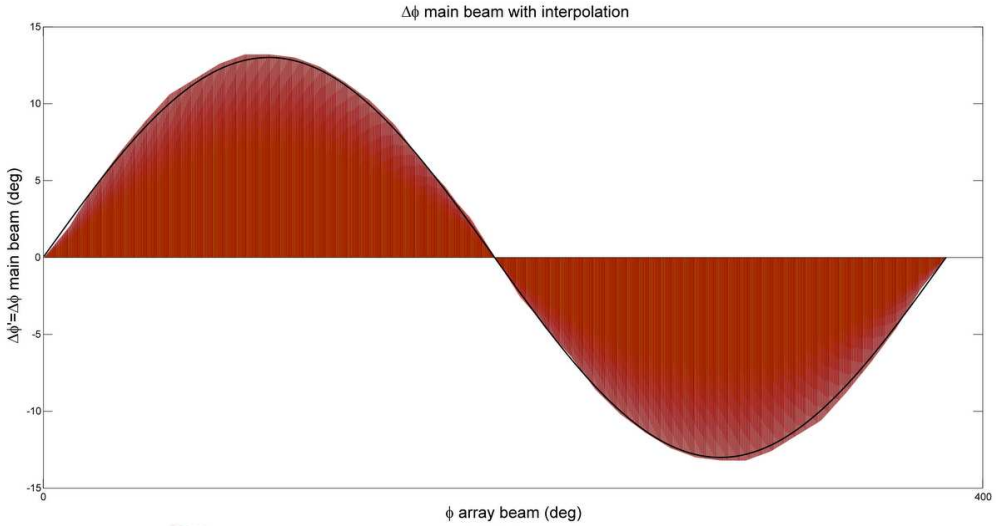

Figure 11. Interpolation for continuous ϕ and fixed $\theta = 26°$ (maximum).

In Figure 10, ϕ is considered to vary in steps of 10° from 0° to 360° and, for each plane individuated by ϕ, θ is varying from 0° to 26° (angle permitting to cover completely the Earth coverage from a geostationary satellite) in steps of 1°.

With a simple interpolation the behaviour can be generalized for each $\Delta\phi'$ (and a fixed θ).

The ideal sinusoidal behavior is underlined in Figure 11 for $\theta = 26°$.

Overall, one may conclude that

$$\Delta\phi' = K1 \sin(\phi) \tag{6}$$

where the quantity $K1$ is clearly a function of θ, M and f/d. Varying θ in steps of 1° (from 0° to 26°) the sinusoidal behavior is confirmed (see Figure 12). Plotting $\Delta\phi'$ (main aperture beam) as a function of the θ of the array (for fixed ϕ), a quasi linear dependence can be appreciated (see Figure 13).

The not perfect linearity of the curves depicted is due to numerical approximation of the BTA. The quantity defined as $K1$, which corresponds to the amplitude of the sinus function individuating the relationship between ϕ' and ϕ, can be derived from the curve corresponding to phi = 90°. For the test configuration proposed ($M = 3$, $f/d = 1.15$), $K1$ is well interpolated by the relation $K1 = 0.51\theta$.

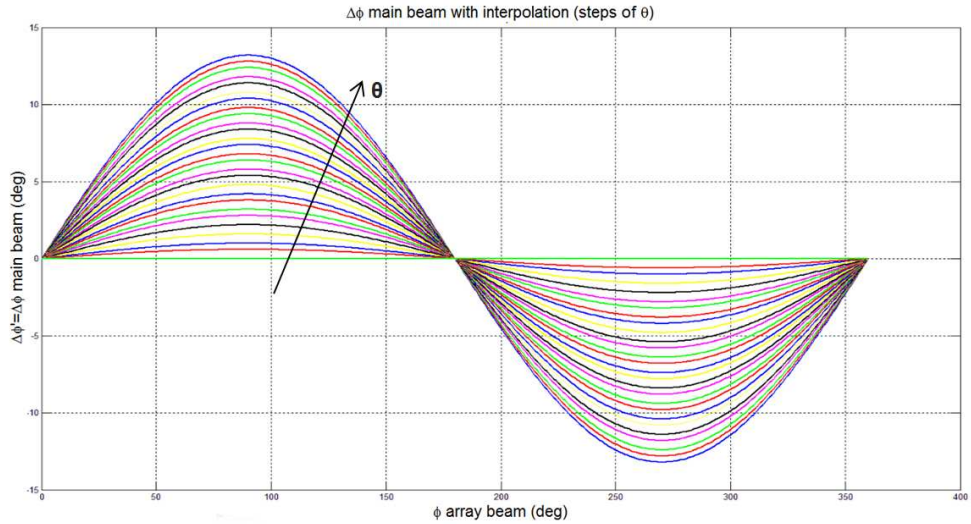

Figure 12. Interpolation showing $\Delta\phi'$ for continuous ϕ and 27 case of θ (from 0° to 26°: step 1°).

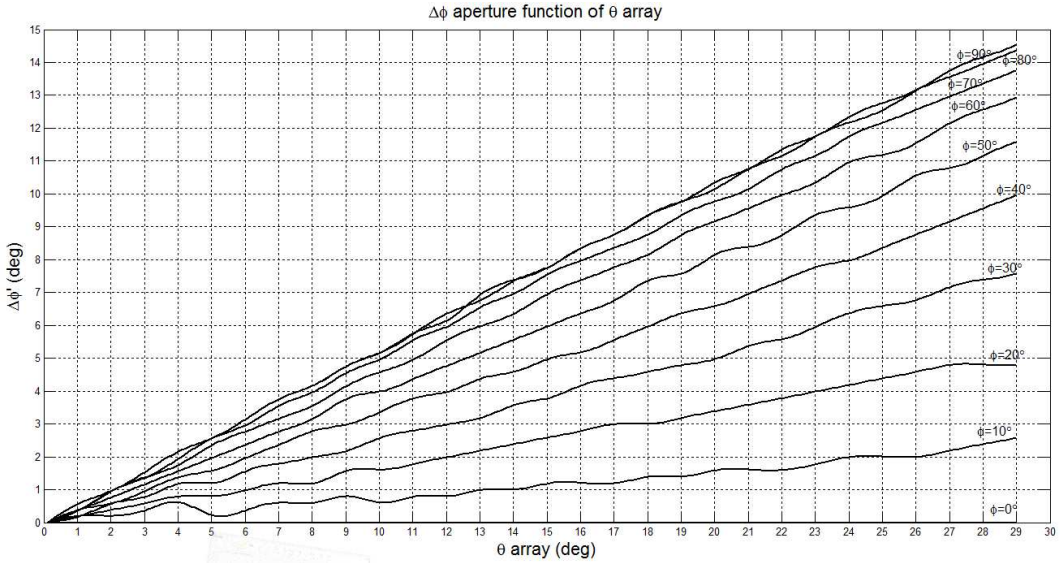

Figure 13. $\Delta\phi'$ function of θ for 10 cases of ϕ (from 0° to 90°; step 10°).

This represents the first of the two relationship which links the real and theoretical directions of main beam scan.

Based on these results, a new improved equation may be presented for the azimuthal scanning properties of the antenna system.

$$\phi' = \phi + \Pi + \Delta\phi' = \phi + \Pi + K1\sin(\phi) \tag{7}$$

Equation (7) represents a generalization of the second equation in (2).

6.2. Variations on θ'

A similar analysis has been implemented in order to characterize $\Delta\theta'$.

A saturation behavior can be observed in Figure 14 in case of up scanning. It is due to the fact that the sub-reflector is exactly dimensioned (see Figure 1) for an Earth coverage (±8°). For up scanning this is achieved with a scan angle of around 21° on the array, while 26°, as already specified,

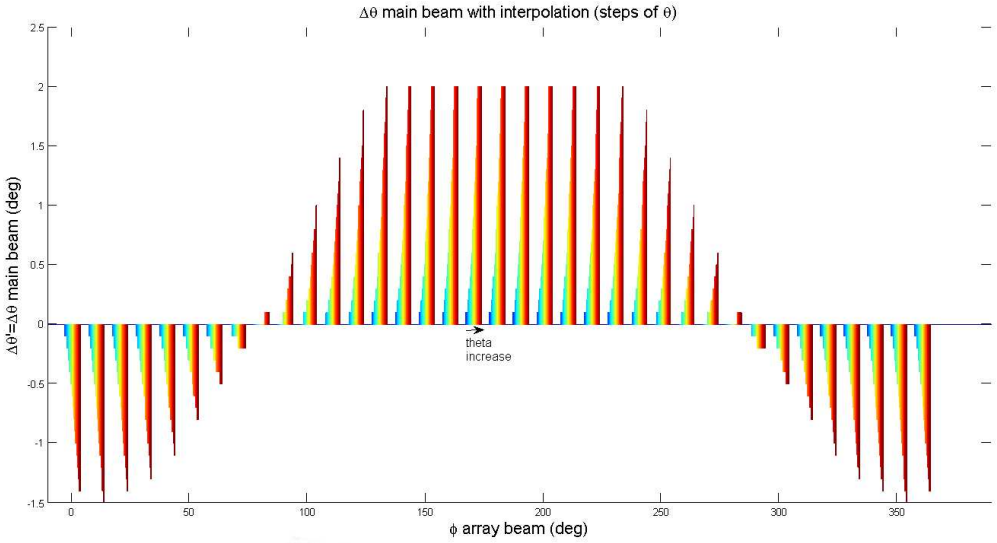

Figure 14. $\Delta\theta'$ as a function of θ and ϕ. θ varies from 0° to 26° (1° step) for every $0° \leq \phi \leq 360°$ (10° step).

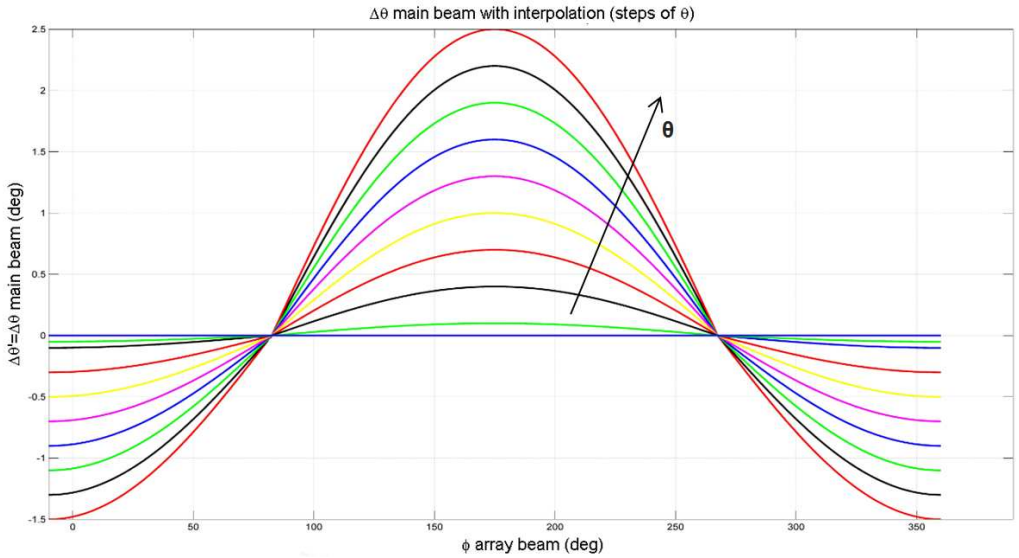

Figure 15. Interpolation showing $\Delta\theta'$ for continuous ϕ and 10 cases of θ (from 0° to 27°, step 3°).

are required only for main scan down. Removing this constraint (which in any case refers to the best system dimensioning), a quick interpolation can be performed on the data. The behavior in Figure 15 is obtained, showing that:

$$\Delta\theta' = K2\cos(\phi + \Pi) \tag{8}$$

where $K2$ is function of θ, M and f/d.

In Figure 15 θ goes up to 27° with a granularity of 3°.

Plotting the $\Delta\theta'$ (main aperture beam) as a function of the θ of the array (see Figure 16), again, a quasi linear behavior is found, although sensibly smoother than for the $\Delta\phi'$. The quantity $K2$ can be derived from the curve corresponding to $\phi = 180°$.

For the present test configuration, the following extrapolation has been derived: $K2 = 0.086\theta$.

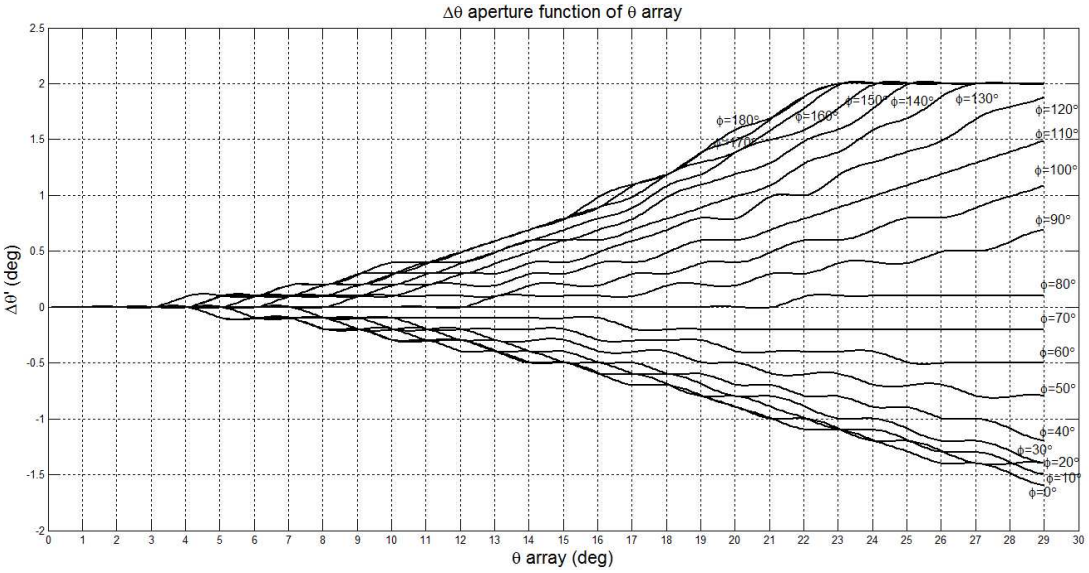

Figure 16. $\Delta\theta'$ function of θ for 19 cases of ϕ (from 0° to 180°; step 10°).

Considering the first equation in (2):

$$\theta' = \frac{1}{M}\theta + \Delta\theta' = \frac{1}{M}\theta + K2\cos(\phi + \Pi) \tag{9}$$

Since smaller variations on $\Delta\theta'$ are obtained (as respect to $\Delta\phi'$), a better accuracy of the BTA is in general needed in this case, as underlined by the ripple in the curves in Figure 16. Nevertheless, this is considered, at present, a point of improvement for the BTA routine, since the actual code would lead to very large computational times. The saturation previously justified is visible also in Figure 16.

7. DEPENDENCE ON M AND f/d

The two characteristic parameters which defines the Dragonian system are the magnification factor (M) and the ratio between focal distance and diameter (f/d). The reference test configuration considered $M = 3$ and $f/d = 1.15$. Nevertheless, a larger set of combination can be deemed suitable for the best optimization of the system with respect to the desired field of applications. Therefore, other solutions were validated with the BTA approach. The method implemented allows to determine easily the coefficients $K1$ and $K2$, depending on the configuration selected (i.e., M and f/d).

The analyses showed, in general, that with lower M higher $K1$ and $K2$ coefficients are obtained. Higher $K1$ and $K2$ coefficients are obtained as well with lower f/d.

In conclusion, the empiric laws derived:

$$\begin{aligned} \Delta\phi' &= K1\sin(\phi) \\ \Delta\theta' &= K2\cos(\phi + \Pi) \end{aligned}$$

allow to redefine the relation in (2) for an offset Dragonian configuration according to:

$$\begin{aligned} \phi' &= \phi + \Pi + a\theta\sin(\phi) \\ \theta' &= \left(\frac{1}{M} + b\cos(\phi + \Pi)\right)\theta \end{aligned} \tag{10}$$

where each of the new angles of the main scan depends on both the angles of the array scan. a and b are two simple scalars derived expliciting θ from $K1$ and $K2$, which depend only on M and f/d.

The analysis of suitable ranges for the two parameters was also part of the study. It has been demonstrated that high values for the magnification factor cause lower distortion, but require higher

scan capabilities for the array feed and imply a reduced compactness so that a trade-off should be performed. Viceversa, there is a higher flexibility in the selection of ratio between focal length and diameter; in practice, the minimum value which guarantees an absence of blockage can be used.

8. CONCLUSIONS

The scanning properties of dual reflector antenna systems constituted by two confocal paraboloidal reflectors fed by a planar array have been investigated. Heuristic equations, representing an extension of the linear equations available in the literature, have been derived which permit predicting the system's pointing direction as a function of the pointing direction of the feeding array in a significant field of view. All the proposed equations may be used for arbitrary configurations with an assigned magnification factor (M) and ratio between focal length and diameter (f/d). It has been verified that the equations are extremely accurate when the system is scanning up to more than 10 beamwidths in all the directions starting from the boresight direction. The validity of the equations remains good even extending further the field of view. However, this extension is, in general for such systems, not recommended because spillover, blockage, cross-polarization effects are seriously affecting the radiative performance.

Further improvements in the control of the radiative performance of this type of antenna system may be obtained by implementing, in addition, other solutions as shaping of one or both reflectors, mechanically modifying the reciprocal positions of the array versus the two reflectors as proposed in [7].

The work has been mainly driven by the recent renewed interest in this type of antenna architecture which may be selected for advanced multibeam satellite applications [8].

REFERENCES

1. Fitzgerald, W. D., "Limited electronic scanning with an offset-feed near-field Gregorian system," ESD-TR-71-272, Technical Report 486, Lincoln Laboratory, 1971.
2. Dragone, C. and M. J. Gans, "Imaging reflector arrangements to form a scanning beam using a small array," *Bell Syst. Tech. J.*, Vol. 58, No. 2, 501–515, 1979.
3. Dragone, C., et al., "Scannable antenna arrangements capable of producing a large image of a small array with minimal aberrations," U.S. Patent 4203105, May 13, 1980.
4. Dragone, C., "Theory of imaging in Cassegrainian and Gregorian antennas," *IEEE Trans. Antennas Propag.*, Vol. 34, No. 5, 689–701, 1986.
5. Pearson, R. A., "An array-fed dual reflector antenna," Ph.D. Thesis, 1988.
6. Rao, J. B. L., "Bicollimated offset Gregorian dual reflector antenna system," U.S. Patent 4755826, Jul. 5, 1998.
7. Martinez-Lorenzo, J. A., A. Garcia-Pino, B. Gonzalez-Valdes, and C. M. Rappaport, "Zooming and scanning Gregorian confocal dual reflector antennas," *IEEE Trans. Antennas Propag.*, Vol. 56, No. 9, Sep. 2008.
8. Gatti, N., A. Catalani, L. Russo, P. Rinous, and G. Toso, "Shaped confocal antenna fed by active sparse array for multibeam satcom applications," *34th ESA Antenna Workshop*, Noordwijk, The Netherlands, 2012.